Supplement of Atmos. Meas. Tech., 17, 6945–6964, 2024
https://doi.org/10.5194/amt-17-6945-2024-supplement

Atmospheric Measurement Techniques
Open Access
EGU

Supplement of

Merging holography, fluorescence, and machine learning for in situ continuous characterization and classification of airborne microplastics

Nicholas D. Beres et al.

Correspondence to: Nicholas D. Beres (nic.beres@dri.edu)

S1 Morphology measures from holographic image analysis

In Sect. 3.1 of the main manuscript, we define several measured parameters of particles derived from the holographic imaging system of the SwisensPoleno. Each holographic particle image is binarized (converted from pixel values ranging from 0 to 1 to a value of either 0 or 1 based on thresholding) and measurements are calculated using the scikit-image image processing software (van der Walt et al., 2014). The measurements discussed in the main text are defined here.

The maximum area-equivalent diameter is defined as the diameter of a circle with the same 2-dimensional projected area as the imaged particle's projected area, where the maximum value of this measurement from the two holographic images is taken. A boxplot showing the distribution of maximum area-equivalent diameters for each class used in the study is shown in Figure S1. The eccentricity is calculated from an ellipse fitted to the measured particle, where the value is the ratio of the distance between focal points of this ellipse to the major axis length of the particle. Major axis lengths of the particle are also derived from the lengths between the focal points of this fitted ellipse; the range of maximum major axis lengths of the particle types in this study is shown in Figure S2. An eccentricity value of zero indicates the particle image is a perfect circle, and as the value approaches 1, the particle is more elongated. Here, again, the maximum of this measurement is taken from the two particle images, and the distributions of the maximum eccentricity measurements for each class is shown in Figure S3. The solidity is calculated by taking the ratio of the area of the convex hull (smallest convex polygon that encloses the particle in the image) to the area of the particle. A solidity value of 1 indicates a "solid" particle outline that is smooth, and values will decrease as the particle in the image becomes more irregular, forming larger "holes" between the convex hull and particle areas. The maximum solidity for each particle class is shown in Figure S4.

S2 Machine learning specifications

In this study, three separate machine learning models were tested for their ability to classify particle type. One convolutional neural network (CNN) model, a multi-layer perceptron (MLP) model, and a third, hybrid model (CNN and MLP) were trained and tested using the Keras (Chollet, 2015) and Tensorflow (Abadi et al., 2016) frameworks in the Python programming were developed. A simplified overview of the model architectures and each layer's output dimensions are shown in Figure S5.

The first model, termed "Holo.-Only," is a convolutional neural network (CNN) that used the two holographic images of a particle as input. Each holographic image used for machine learning is 200x200 pixels, with 16 bits per pixel, with pixel values ranging from 0 to 1. To enhance both model performance and training efficiency, we employ transfer learning—a method enabling the application of a pretrained model from one data domain to a similar one without extensive retraining (Weiss et al., 2016). We utilize the EfficientNet B0 model (Tan and Le, 2019), previously trained on the ImageNet image database. This model requires an RGB image input (width x height x 3), with pixel values ranging from 0 to 255. Consequently, holographic images are stacked to create a 200x200x3, matching the necessary EfficientNet input layer, followed by mapping

pixel values to the 0-255 data range. Each holographic image is used with an EfficientNet B0 layer, and their resultant outputs (7x7x1280) are concatenated (7x7x2560) and flattened (1x125440) prior to the final model layers. This model had 5,931,186 total parameters, of which 1,881,615 were trainable in this application.

We utilized an MLP model which used only the relative fluorescence spectra from the SwisensPoleno as input ("Fl.-Only"). These data have dimensions 1x13, representing the 13 measured fluorescence combinations of excitation sources and emission wavebands for each event. For this model, the relative fluorescence values are also mapped to the 0 to 255 data domain and the passed through three fully connected dense layers (with depths of 1024, 64, and 16 nodes, respectively), each with the Rectified Linear Unit (ReLU) activation function. The output from the final dense layer is passed to the final model layers. This model had a total of 47,919 parameters, all of which were trainable.

The third model used the two holographic images and relative fluorescence spectra as input ("Holo.+Fl."). This multi-input model is a hybrid structure that utilizes components and architecture from the two previously described CNN and MLP models. For this hybrid model, the outputs from each of the two previously described models (1x125440 for the Holo.-Only model and 1x16 for the Fl.-Only model) are concatenated together before the final model layers, for which all three models are the same. This model had a total parameter count of 5,979,090, of which 1,929,519 were trainable.

Each of the three models shared the final model layers and training configurations. The final model layers common to all three model variants pass the output from each model through a 30% dropout layer (Hinton et al., 2012) before a final dense layer with linear activation and dimensions matching that of the number of classes used in the model. Finally, a Softmax activation layer provided the probability distribution of classification prediction certainty across tested classes. Each model utilized the Adam optimizer (Kingma and Ba, 2014) with a learning rate $\eta=5e^{-6}$ and minimized the cross-entropy loss between predicted and true model outputs.

Prior to model training, the full dataset (142,072 events) was split randomly along a 60/40% split for training and testing, respectively; the same training and testing datasets were used across all three model architectures. The Holo.-Only model was trained for 80 epochs, the Fl.-Only model was trained for 150 epochs, and the combined Holo.-Fl. model was trained for 40 epochs. During model inference, the predicted class is chosen as the maximum of the Softmax distribution based on input data from the validation dataset. The accuracy reported throughout the study is the computed harmonic mean between the precision and recall of the model evaluation, also known as the f-score, where a value closer 1 indicates better model performance; detailed information about these evaluation metrics can be found in (Müller and Guido, 2016).

S3 Overview of the SwisensPoleno fluorescence measurement system

The SwisensPoleno system utilizes advanced fluorescence spectroscopy to analyze individual airborne particles. This system is equipped with multiple excitation sources and emission detectors, referred to here as wavebands, facilitating a comprehensive spectral analysis of particles.

The SwisensPoleno measures individual particle fluorescence emissions in five wavebands (with center wavelengths at 357 nm, 435 nm, 483 nm, 562 nm, 676 nm) using silicon photomultipliers (SiPMs) with optical filters according to the measurement wavebands. There are three excitation sources, where each particle is excited by a 365 nm LED, a 280 nm LED, and a 405 nm laser diode, sequentially. These light sources are intensity modulated between 10 and 60 MHz to induce phase shifts and demodulation cause by fluorescence lifetimes in the nanosecond range; however, fluorescence lifetime data for each particle are not utilized in this study. Instead, for this work, only the mean intensity per excitation source and waveband, with stray light already subtracted, is considered, providing an absolute fluorescence intensity spectrum for each particle.

Because pure water is not expected to fluoresce, any detectable fluorescence signal from the pure water droplets represents measurement noise. To separate actual fluorescence from noise, an intensity threshold is used, defined as a factor of the standard deviation of water droplets. With the signal standard deviation of water σ_{water} , the threshold θ_{FL} was defined as:

$$\theta_{FL} = 3.5 \cdot \sigma_{water}$$

The factor of 3.5 sets the threshold significantly higher than the background fluorescence signal of water droplets measured by the SwisensPoleno, defining a robust condition for distinguishing fluorescent particles from non- or very weakly fluorescent particles. Changing the factor may affect the portion of excluded events from analysis and machine learning trainings, but only for very weakly fluorescent particles.

Fluorescence measurements should ideally depend only on the composition of the detected particle. Differences, however, arise in absolute fluorescence intensity dependent on particle size, location within the measurement volume, or small differences in instrument excitation and detection capabilities and optical arrangement. These factors also make comparisons between instruments more difficult. To address these issues, the measured absolute fluorescence intensity of each waveband in the SwisensPoleno is normalized by the sum of all five waveband intensities for each excitation source, providing a measured relative fluorescence spectrum that varies from 0 to 1. Similarly defined in Erb et al. (2024), the relative fluorescence intensity $r_{i,j}$ for waveband i and excitation source j is defined as the ratio of the absolute fluorescence intensity $a_{i,j}$ to the sum of fluorescence intensities across all wavebands k for the same excitation source j. That is:

$$r_{i,j} = \frac{a_{i,j}}{\sum_k a_{k,j}}$$

The calculation of the relative fluorescence also ensures transferability between different SwisensPoleno instruments, such as the array used in the Swiss automatic pollen monitoring network at the Federal Office of Meteorology and Climatology in Switzerland, MeteoSwiss.

References

Abadi, M., Barham, P., Chen, J., Chen, Z., Davis, A., Dean, J., Devin, M., Ghemawat, S., Irving, G., Isard, M., and others: Tensorflow: a system for large-scale machine learning., in: Osdi, 265–283, 2016.

Chollet, F.: Keras, 2015.

Erb, S., Graf, E., Zeder, Y., Lionetti, S., Berne, A., Clot, B., Lieberherr, G., Tummon, F., Wullschleger, P., and Crouzy, B.: Real-time pollen identification using holographic imaging and fluorescence measurements, Atmos Meas Tech, 17, 441–451, https://doi.org/10.5194/amt-17-441-2024, 2024.

Hinton, G. E., Srivastava, N., Krizhevsky, A., Sutskever, I., and Salakhutdinov, R. R.: Improving neural networks by preventing co-adaptation of feature detectors, 1–18, 2012.

Kingma, D. P. and Ba, J.: Adam: A Method for Stochastic Optimization, 3rd International Conference on Learning Representations, ICLR 2015 - Conference Track Proceedings, 1–15, 2014.

Müller, A. C. and Guido, S.: Introduction to Machine Learning with Python, O'Reilly Media, Inc., 2016.

Tan, M. and Le, Q. V.: EfficientNet: Rethinking model scaling for convolutional neural networks, 36th International Conference on Machine Learning, ICML 2019, 2019-June, 10691–10700, 2019.

van der Walt, S., Schönberger, J. L., Nunez-Iglesias, J., Boulogne, F., Warner, J. D., Yager, N., Gouillart, E., and Yu, T.: scikit-image: image processing in Python, PeerJ, 2, e453, https://doi.org/10.7717/peerj.453, 2014.

Weiss, K., Khoshgoftaar, T. M., and Wang, D. D.: A survey of transfer learning, Springer International Publishing, https://doi.org/10.1186/s40537-016-0043-6, 2016.

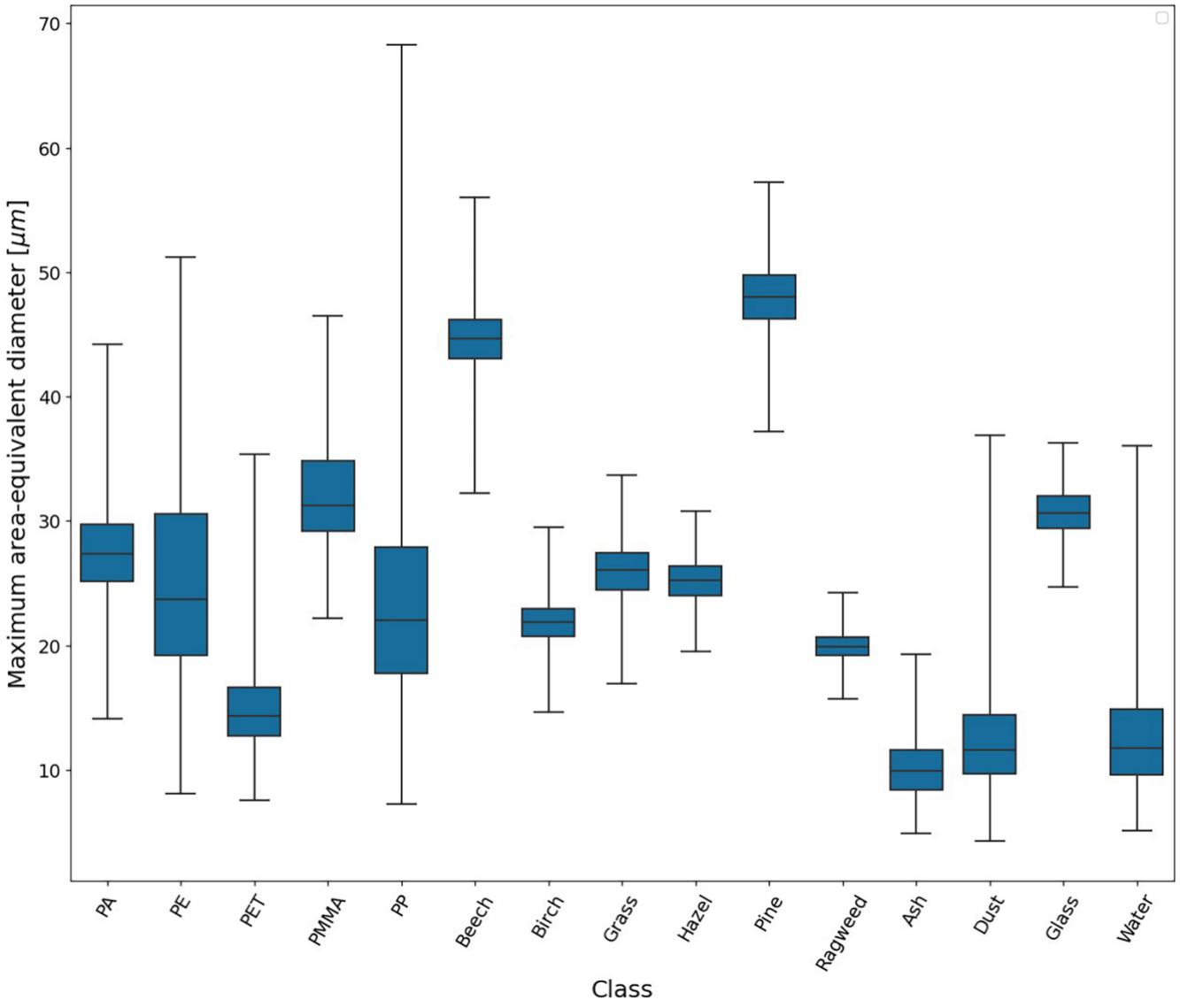

Figure S1: A boxplot showing the maximum area-equivalent diameters for all events used in this study. The box indicates the quartiles of each class dataset, and the whiskers show the full range of the dataset.

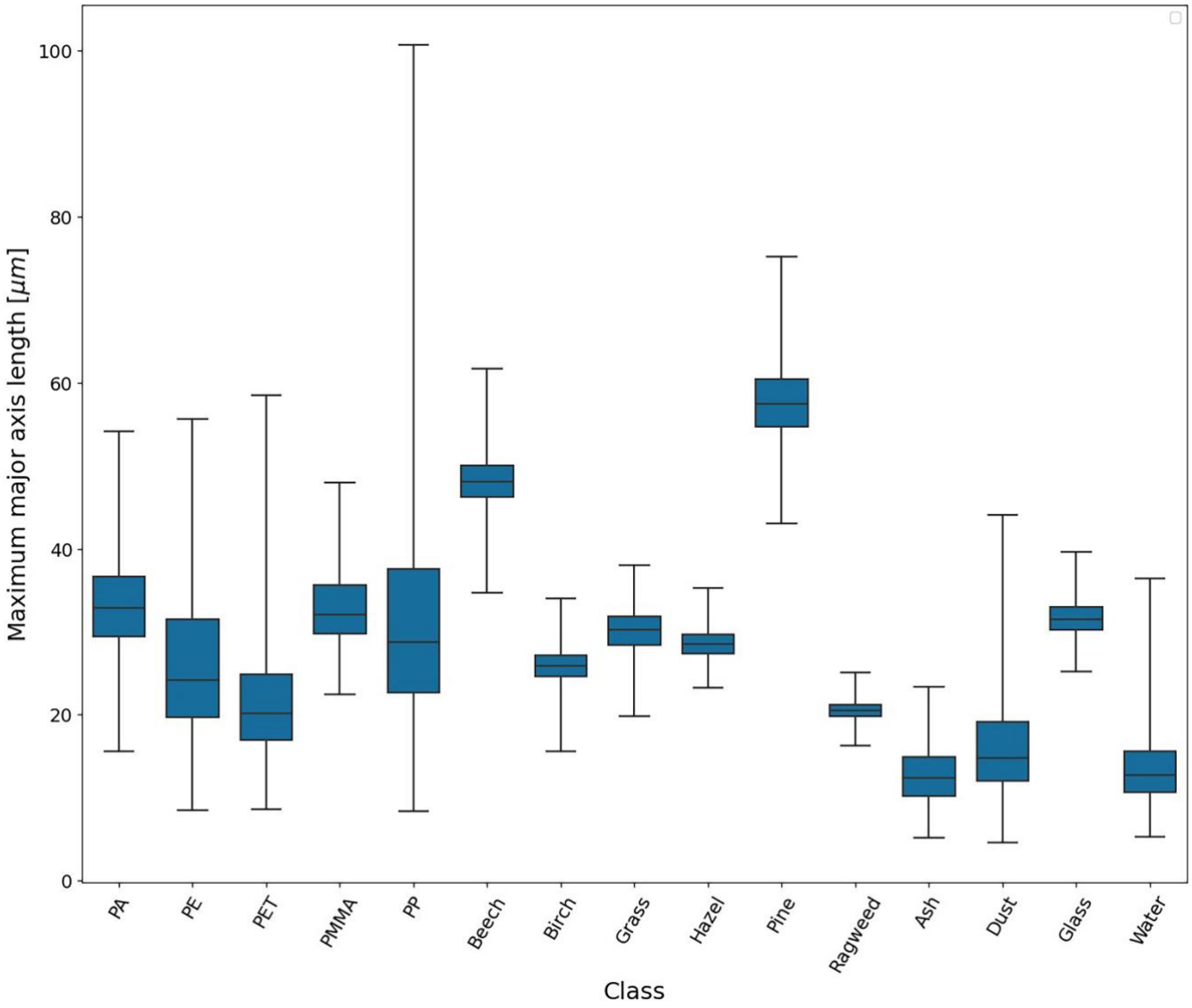

Figure S2: A boxplot showing the maximum major axis length for all events used in this study. The box indicates the quartiles of each class dataset, and the whiskers show the full range of the dataset.

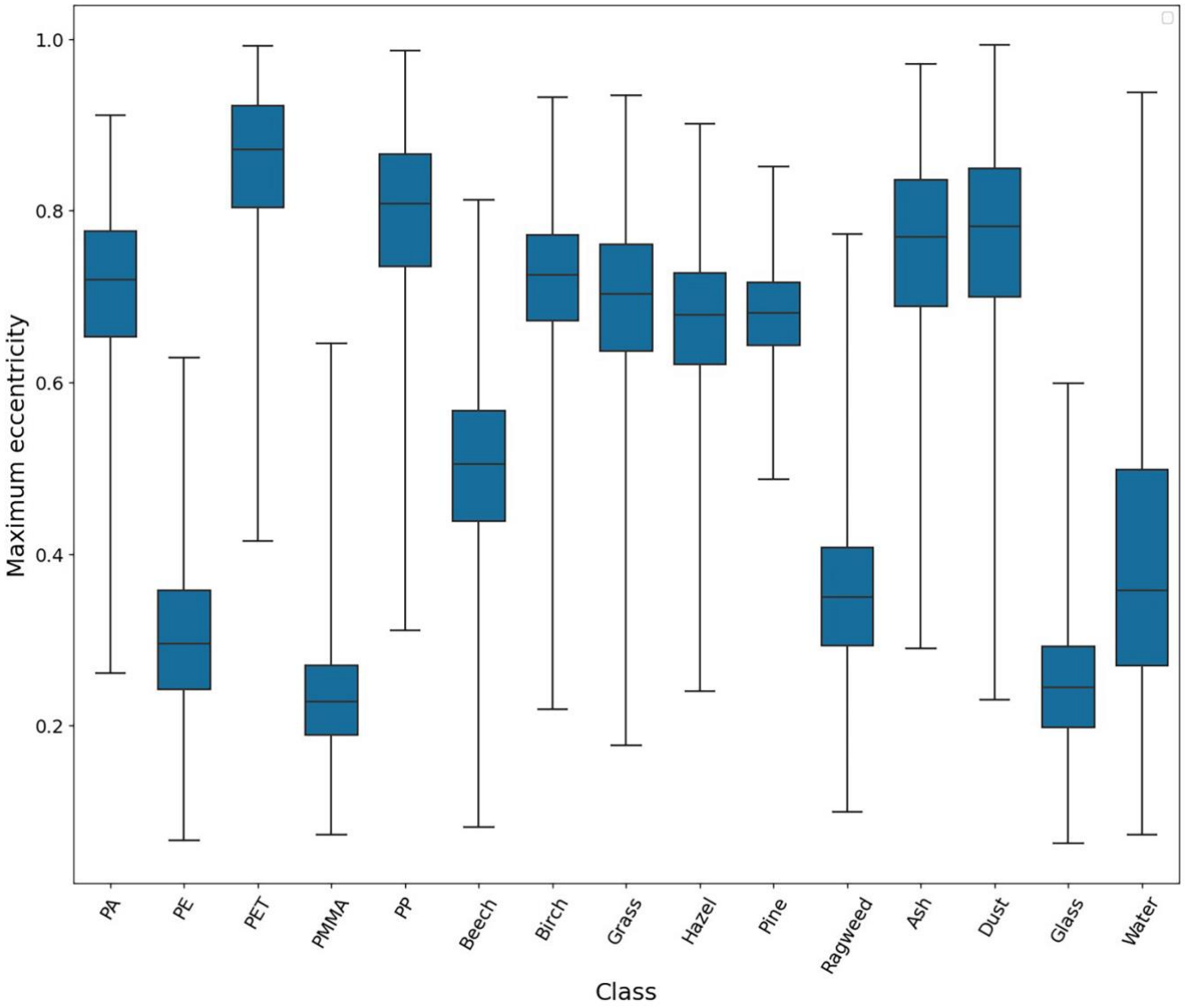

Figure S3: A boxplot showing the maximum eccentricity for all events used in this study. The box indicates the quartiles of each class dataset, and the whiskers show the full range of the dataset.

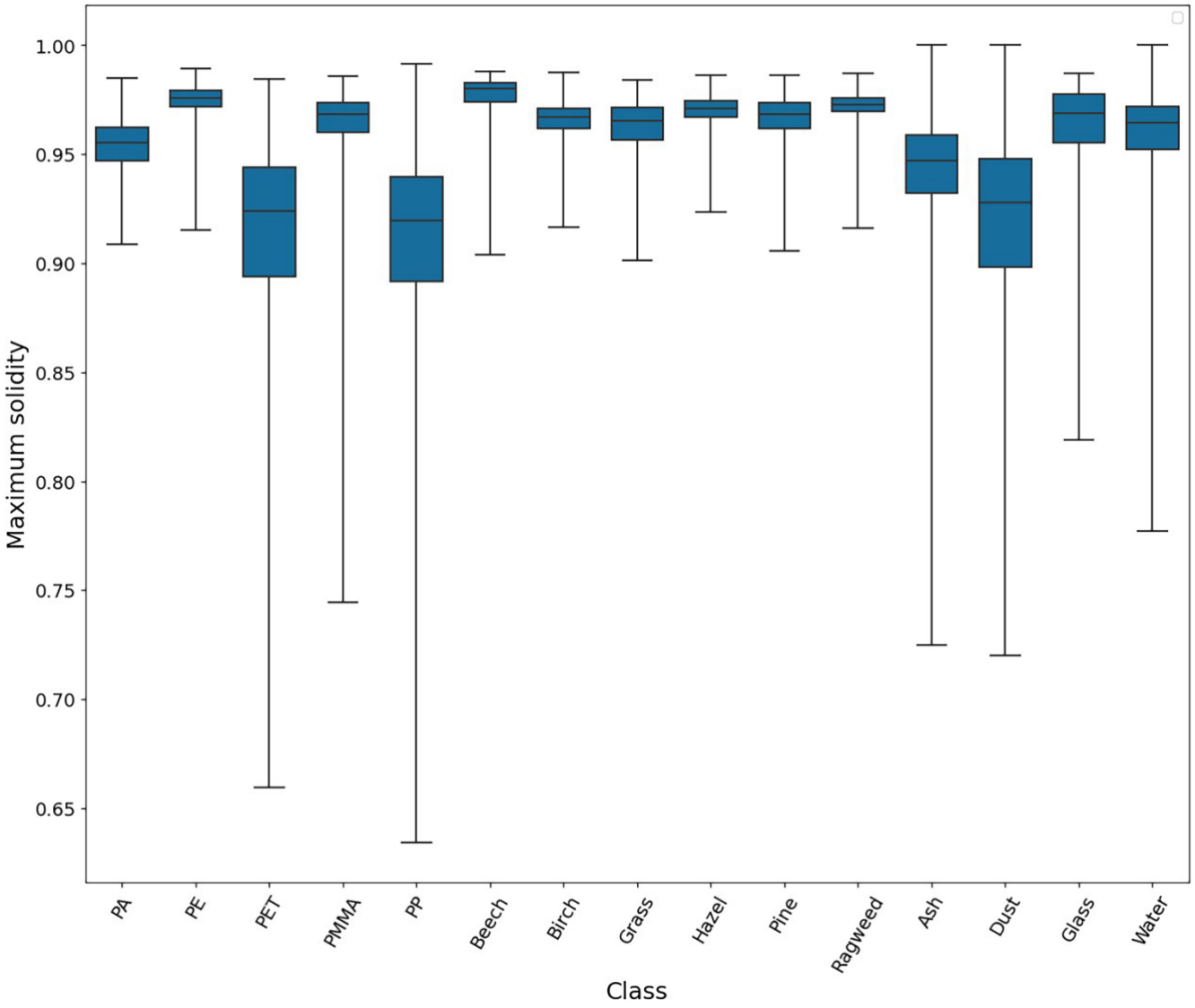

Figure S4: A boxplot showing the maximum solidity measurement for all events used in this study. The box indicates the quartiles of each class dataset, and the whiskers show the full range of the dataset.

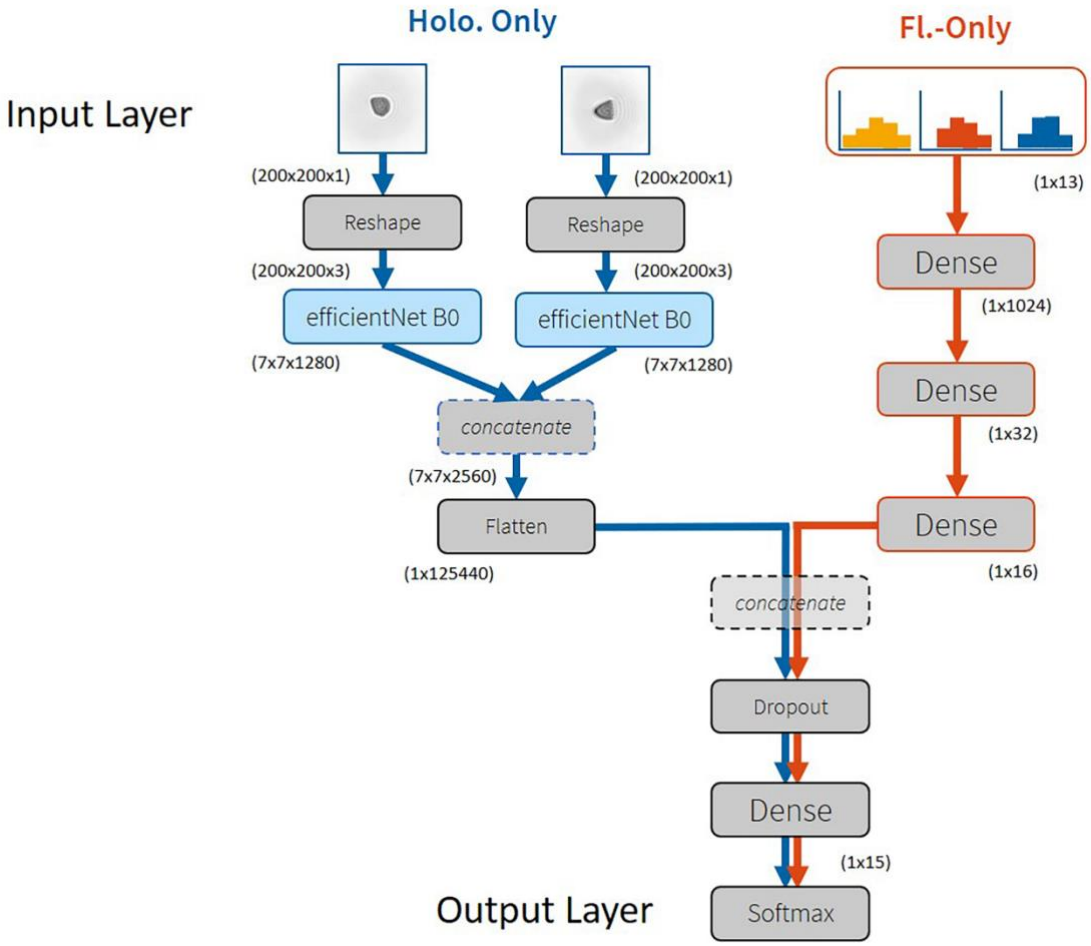

Figure S5: Machine learning model architecture for the study, where numbers indicate the previous layer's output dimensions. Three different model architectures are used with this existing structure. The left path ("Holo.-Only", colored blue) uses only the two holographic images as input. The right path ("Fl.-Only", colored red) uses only the relative fluorescence spectra, here depicted as a plot of relative intensities. The third model combines both the two holographic images and the relative fluorescence spectra, which are concatenated together. The output layer is the Softmax prediction probability output, which classifies particle type by taking the maximum of this output. Here, as an example, the holographic image inputs and relative fluorescence spectra plot represent a single hazel pollen event.